

1 **The underappreciated impact of emission source profiles on the simulation of**
2 **PM_{2.5} components: New evidence from sensitivity analysis**

3 Zhongwei Luo^{a,b,1}, Yan Han^{a,b,c,1}, Kun Hua^{a,b}, Yufen Zhang^{a,b*}, Jianhui Wu^{a,b}, Xiaohui
4 Bi^{a,b}, Qili Dai^{a,b}, Baoshuang Liu^{a,b}, Yang Chen^c, Xin Long^c, Yinchang Feng^{a,b*}

5 ^aState Environmental Protection Key Laboratory of Urban Ambient Air Particulate
6 Matter Pollution Prevention and Control & Tianjin Key Laboratory of Urban
7 Transport Emission Research, College of Environmental Science and Engineering,
8 Nankai University, Tianjin 300350, China.

9 ^bCMA-NKU Cooperative Laboratory for Atmospheric Environment-Health Research,
10 Tianjin 300350, China.

11 ^cResearch Center for Atmospheric Environment, Chongqing Institute of Green and
12 Intelligent Technology, Chinese Academy of Sciences, Chongqing 400714, China.

13

14

15 *Corresponding authors:

16 Y. F. Zhang (zhafox@nankai.edu.cn). And Y. C. Feng (fengyc@nankai.edu.cn).

17

18 ¹Z. W. Luo and Y. Han equally contribute to this work

19 **Abstract**

20 The chemical transport model (CTM) is an essential tool for air quality prediction
21 and management, widely used in air pollution control and health risk assessment.
22 However, the current models do not perform very well in simulating PM_{2.5} components.
23 Studies suggested that the uncertainties of model chemical mechanism, source emission
24 inventory and meteorological field can cause inaccurate simulation results. Still, the
25 emission source profile of PM_{2.5} has not been fully taken into account in current
26 numerical simulation. This study aims to answer (1) Whether the variation of source
27 profile adopted in CTMs has an impact on the simulation of PM_{2.5} chemical components?
28 (2) How much does it impact? (3) How does the impact work? Based on the
29 characteristics and variation rules of chemical components in typical PM_{2.5} sources,
30 different simulation scenarios were designed and the sensitivity of components
31 simulation results to PM_{2.5} sources profile was explored. Our findings showed that the
32 influence of source profile changes on simulated PM_{2.5} concentration was insignificant,
33 but its impact on PM_{2.5} components could not be ignored. The variations of simulated
34 components ranged from 8% to 167% under selected different source profiles, and
35 simulation results of some components were sensitive to the adopted PM_{2.5} source
36 profile in CTMs. These influences are connected to the chemical mechanisms of the
37 model since the variation of species allocations in emission sources directly affected
38 the thermodynamic equilibrium system. We also found that the perturbation of the PM_{2.5}
39 source profile caused the variation of simulated gaseous pollutants, which indirectly
40 indicated that the perturbation of the source profile affected the simulation of secondary
41 PM_{2.5} components. Given the vital role of air quality simulation in environment
42 management and health risk assessment, the representativeness and timeliness of source
43 profile should be considered.

44 **Keywords**

45 PM_{2.5}; source profile; component; numerical simulation; chemical transport model

46 **1. Introduction**

47 Ambient fine particulate matter (PM_{2.5}) pollution in some key regions of China
48 has attracted much attention (Liang et al., 2020; Huang et al., 2021). The chemical
49 components of PM_{2.5}, including elements (Al, Si, Fe, Mn, Ti, Cu, Zn, Pb, etc.), water-
50 soluble ions (SO₄²⁻, NO₃⁻, Cl⁻, F⁻, NH₄⁺, Na⁺, K⁺, Mg²⁺, Ca²⁺, etc.), and carbon-
51 containing components (Organic Carbon, OC; Elemental Carbon, EC) (Yang et al.,
52 2011; Li et al., 2013), have different physical and chemical properties, such as reactivity,
53 thermal stability, particle size distribution, residence time, optical properties, health
54 hazards, etc (Seinfeld and Pandis, 2006; Tang et al., 2006). According to long-term
55 monitoring results, in most regions of China, SO₄²⁻, NO₃⁻, NH₄⁺ and OC are the most
56 important species in ambient PM_{2.5} (Li et al., 2017a; Li et al., 2021), which has a certain
57 adverse impact on human health (Shi et al., 2018) and ecosystem, such as acid rain in
58 southwest China (Han et al., 2019), food security (Zhou et al., 2018), etc.

59 The chemical transport models (CTMs) play an important role in policy making
60 for regulatory purposes. Based on the scientific understanding of atmospheric physical
61 and chemical processes, CTMs are built to simulate the transport, reaction and removal
62 of pollutants on a certain scale in horizontal and vertical directions. With the
63 development of CTMs, the simulation accuracy of PM_{2.5} concentration has been
64 significantly improved. Higher requirements have been put forward for the precise
65 simulation of PM_{2.5} components so as to provide support for the use of CTMs in human
66 health risk assessment, climate effects, pollution sources apportionment, and so on
67 (Peterson et al., 2020; Lv et al., 2021). However, the current models perform not very
68 well in simulating some components (for example, PM_{2.5}-bound sulfate, nitrate,
69 ammonium, trace elements, etc.) (Zheng et al., 2015; Fu et al., 2016; Ying et al., 2018;
70 Cao et al., 2021). In the current literature, the correlation coefficient (R) and normalized
71 mean bias (NMB) are highly variable and inconsistent between the simulated and the
72 observed values (listed in Table S1). This is mainly attributable to the uncertainties of
73 model chemical mechanism, source emission inventory and meteorological field

74 simulation.

75 The chemical mechanisms involved in CTMs are derived from parameterized
76 assumptions based on laboratory simulation and field observations. The actual
77 atmospheric chemical processes are very complex, and some reaction mechanisms are
78 still limitedly understood. In addition, the integration of chemical reactions and
79 simplified treatment methods in the model cannot fully reflect the correlation among
80 atmospheric pollutants. For example, in some model mechanisms, other important
81 sulfate and nitrate formation pathways were added through new heterogeneous
82 chemistry, including the chemical reaction between SO_2 and aerosol, $\text{NO}_2/\text{NO}_3/\text{N}_2\text{O}_3$
83 and aerosol (Zheng et al., 2015), nitrous acid oxidized SO_2 to produce sulfate (Zheng
84 et al., 2020), dust particles promoted the oxidation of SO_2 (Yu et al., 2020), modified
85 the uptake coefficients for heterogeneous oxidation of SO_2 to sulfate (Zhang et al.,
86 2019), updated the heterogeneous N_2O_5 parameterization (Foley et al., 2010). Even
87 though the aforementioned processes can significantly improve the simulation of SO_4^{2-}
88 and NO_3^- , there is still a gap between the modeled and the actual atmospheric chemical
89 processes.

90 The uncertainty of source emission inventory also significantly affects the
91 simulation results of $\text{PM}_{2.5}$ components (Shi et al., 2017; Sha et al., 2019). Due to
92 incomplete information or insufficient representativeness, pollutant emissions are
93 sometimes overestimated or underestimated, and the method for temporal and spatial
94 allocation also needs to be improved.

95 The uncertainty of meteorological field simulation is another crucial reason for the
96 simulation deviation, especially on heavy pollution days, the variation trends of $\text{PM}_{2.5}$
97 chemical components were not well-captured (Ying et al., 2018; Qi et al., 2019; Wang
98 et al., 2022). Precipitation is the key meteorological factor determining wet removal of
99 pollutants; boundary layer height and wind speed are the main factors affecting
100 convection and transport of pollutants; solar radiation, temperature and relative
101 humidity are the key factors affecting the formation of secondary particles (Huang et
102 al., 2019; Chen et al., 2020). Some literature reported that deviation from precipitation

103 and wind field simulation might lead to underestimation of SO_4^{2-} , NO_3^- and NH_4^+
104 (Cheng et al., 2015; Zhang et al., 2017). Devaluation of liquid water path and cloud
105 cover cause a decrease of sulfate formation in cloud, and ultimately results in
106 significantly underestimated components in simulation values (Sha et al., 2019; Foley
107 et al., 2010). Underestimation of temperature and relative humidity may also cause
108 adverse effects of temperature- and/or relative humidity-dependence chemical reaction
109 in the simulation (Sha et al., 2019).

110 In particular, the emission source profile of $\text{PM}_{2.5}$ (Hereinafter referred to as
111 "source profile"), creating speciated emission inventories for CTMs (Hsu et al., 2019),
112 has not been fully taken into account in the current numerical simulation. In the reported
113 literature, $\text{PM}_{2.5}$ species allocation coefficients of emission sources are commonly
114 treated in the following ways: (1) allocated $\text{PM}_{2.5}$ components of source emissions by
115 referring to source profile data in published literature or database like the US
116 SPECIATE (Fu et al., 2013; Wang et al., 2014; Ying et al., 2018); (2) chemical profiles
117 come from local measurement (Fu et al., 2013; Appel et al., 2013). However, with the
118 development of production technology and the innovation of pollution treatment
119 technology in recent years, some source profiles have changed dramatically (Bi et al.,
120 2019), such as SO_4^{2-} from coal burning, SO_4^{2-} content in $\text{PM}_{2.5}$ is generally low in coal-
121 fired power plant without desulfurizing facilities, while existing coal-fired power plants
122 using limestone/gypsum wet desulphurization, the contents of SO_4^{2-} in $\text{PM}_{2.5}$ are
123 significantly higher than that without desulfurization facilities (Zhang et al., 2020). The
124 timeliness of $\text{PM}_{2.5}$ species allocation coefficients in current CTMs also needs to be
125 considered.

126 This paper attempts to answer the following questions: (1) Whether the variation
127 of the source profile adopted in the air quality model has an impact on the simulated
128 results of $\text{PM}_{2.5}$ chemical components? (2) How much does it impact? (3) How does
129 the impact work? Aiming at these problems above, chemical composition and its
130 variation law for typical $\text{PM}_{2.5}$ emission sources are summarized, on this basis,
131 sensitivity tests are designed to identify whether $\text{PM}_{2.5}$ source profiles and species

132 allocation in the model are important parameters that affect the simulation results of
133 chemical components in PM_{2.5}. We take CMAQ (one of the most widely used CTMs),
134 MEIC (a high-resolution inventory of anthropogenic air pollutants in China) as the
135 carriers. The same kind of experiment is also applicable to other CTMs and emission
136 inventories. The aim of this study is to provide support for the effective utilization of
137 source profiles in the CTMs and improvement of the simulation schemes.

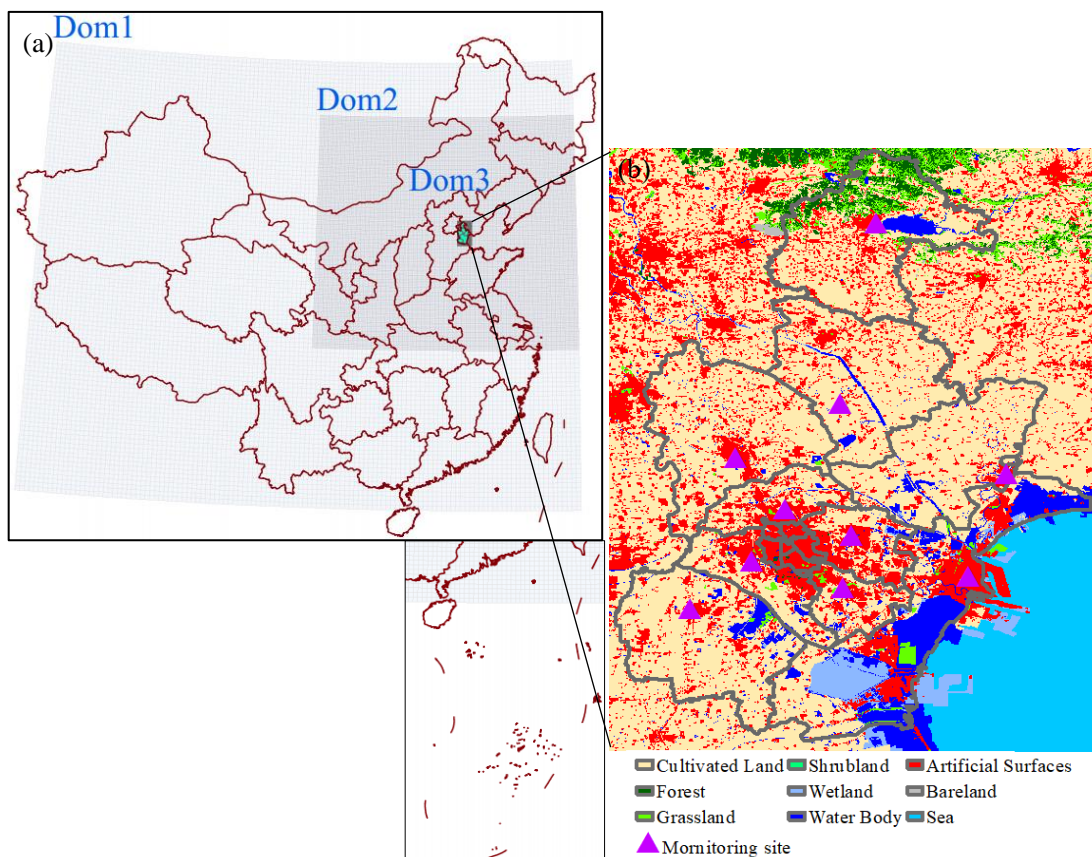
138 **2. Model and Data**

139 **2.1 Model configuration**

140 Weather Research and Forecasting model (WRF-3.7.1), the widely used
141 Community Multiscale Air Quality model (CMAQv5.0.2), and Multi-resolution
142 Emission Inventory for China (MEICv1.3) have been used in this study. MEIC provided
143 the emission inventory which is developed by Tsinghua University, mainly tracked
144 anthropogenic emissions in China including coal-fired power plants, industry, vehicles,
145 residents and agriculture (http://meicmodel.org/?page_id=135) (Li et al., 2017b; Zheng
146 et al., 2018). The WRF model was used to generate meteorological inputs for the
147 CMAQ model. Three nested modeling domains consisting of 36 km×36 km (Dom1),
148 12 km×12km (Dom2), and 4 km×4km (Dom3) horizontal grid sizes were set, as shown
149 in Fig. 1. The initial and boundary conditions for WRF were based on the North
150 American Regional Reanalysis data archived at National Center for Atmospheric
151 Research (NCAR). In addition, surface and upper air observations obtained from
152 NCAR were used to further refine the analysis data. The major configurations we used
153 in CMAQ were illuminated as follows: Gas-phase chemistry was based on the CB05
154 mechanism and the aerosol dynamics/chemistry was based on the aero6 module
155 (cb05tucl_ae6_aq). The detailed model configurations were shown in Table S2,
156 regional distribution of PM_{2.5} emission sources were shown in Fig. S2.

157

158



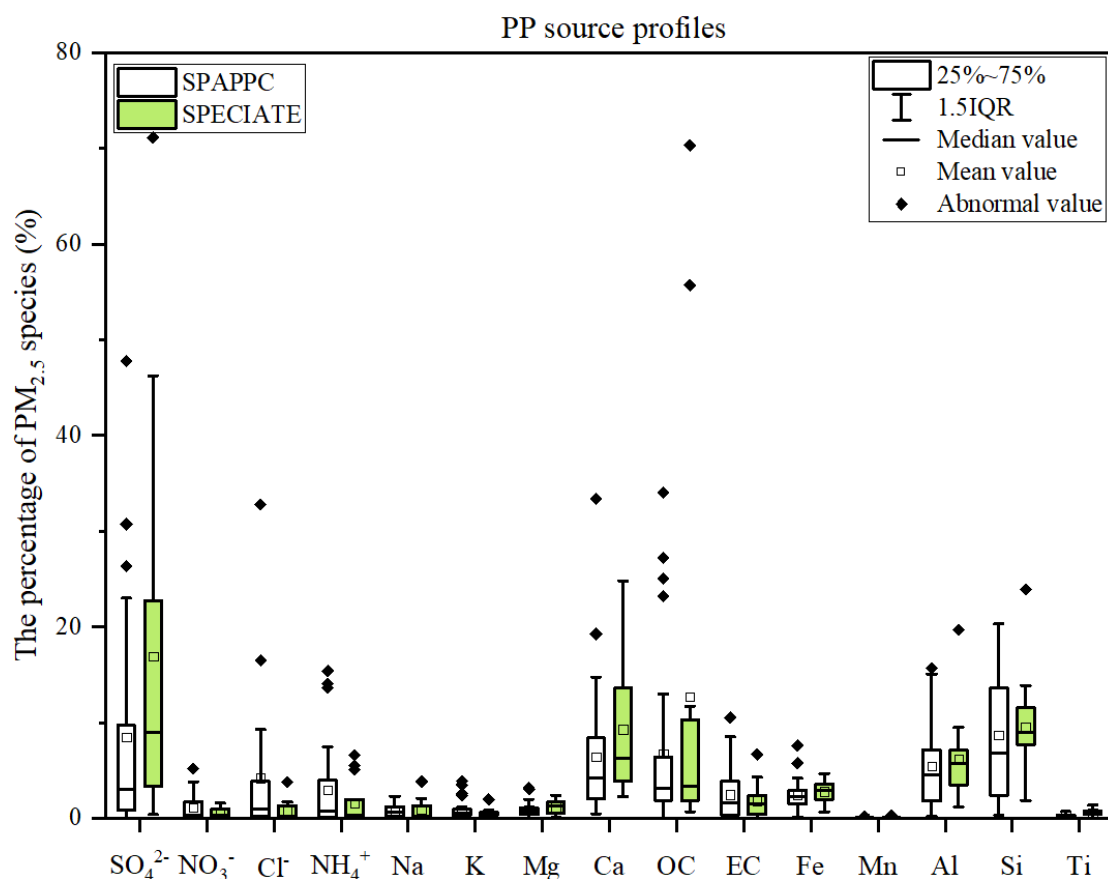
159
 160 Fig.1 Modeling domains of the CMAQ model. (a) The three-domain nested CMAQ domains; (b)
 161 Land use and observation sites of Dom3 (Data source of Land use: GLOBELAND30,
 162 www.globeland30.org, National Geomatics Center of China).

163 2.2 Selection and comparison of PM_{2.5} source profile

164 The PM_{2.5} emission source profiles from database of Source Profiles of Air
 165 Pollution (SPAP) (<http://www.nkspap.com:9091/>), U.S. Environmental Protection
 166 Agency's (EPA) SPECIATE database ([https://www.epa.gov/air-emissions-](https://www.epa.gov/air-emissions-modeling/speciate)
 167 modeling/speciate) as well as from published literature were selected, respectively. The
 168 SPAP was developed by the State Environment Protection Key Laboratory of Urban
 169 Particulate Air Pollution Prevention, Nankai University, China. This database contains
 170 more than 3000 size-resolved source profiles of stationary combustion sources,
 171 industrial processes, vehicle exhaust, biomass burning, dust and cooking emissions and
 172 other sources, collected from more than 40 cities in China since 2001. In addition to
 173 inorganic elements, water-soluble ions, OC, EC and other conventional components,
 174 some source profiles also encompass a series of tracer information, such as organic
 175 markers, isotopes, single particle mass spectrometry, VOCs and other gaseous

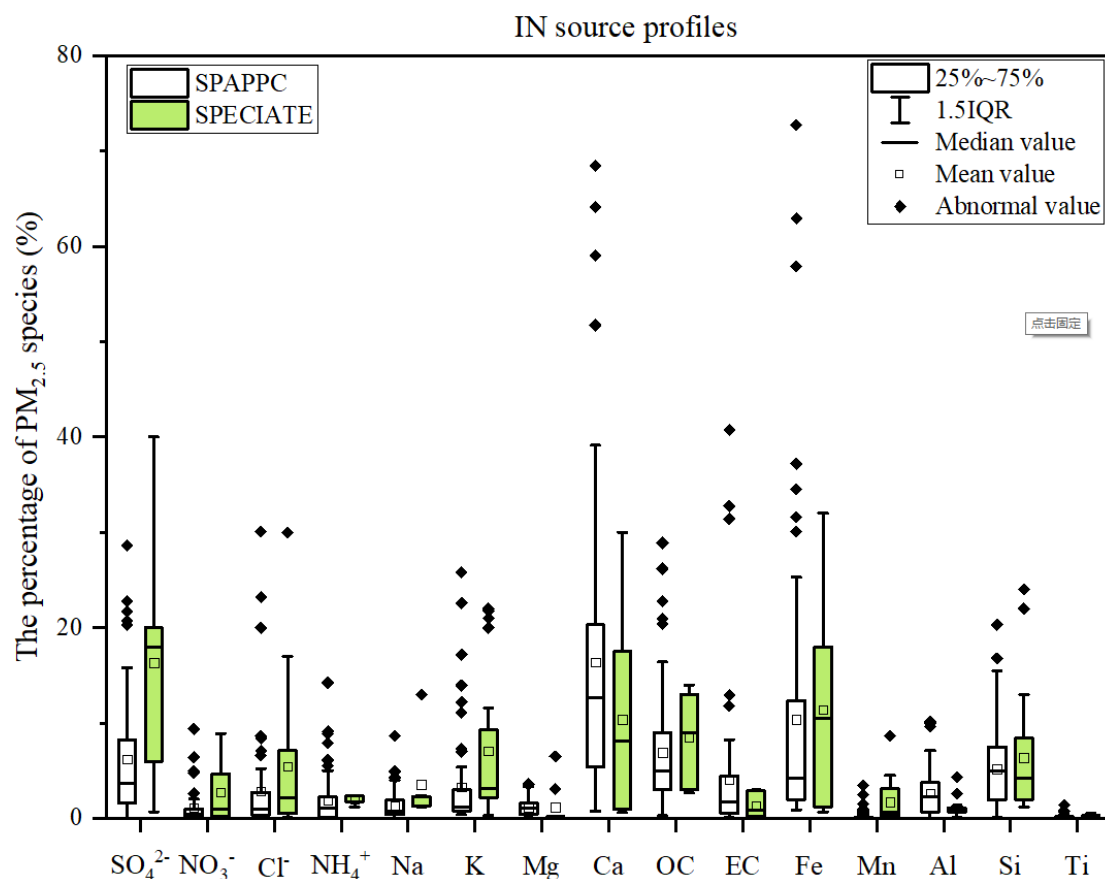
176 precursors. Based on species in the aerosol chemical mechanism (AERO6) (Appel et
177 al., 2013; Chapel Hill, 2012), we selected 15 components in PM_{2.5} source profiles
178 including Al, Ca, Cl, EC, Fe, K, Mg, Mn, Na, OC, Si, Ti, NH₄⁺, NO₃⁻ and SO₄²⁻, the
179 remaining components are classified as “other”. Emission sources are divided into four
180 main categories referred to the classification in MEIC: coal combustion by power plants
181 (PP), industrial processes (IN), residential emission (RE) and transportation sector (TR).

182 Coal-fired power plants remain the main coal consumers in China, which
183 accounted for 50.2% of total coal consumption in 2019 (NBS, 2021) and gained much
184 more attention (Wu et al., 2022), especially with the wide implementation of the
185 strictest ultralow emission standards, PM_{2.5} emission characteristics have changed
186 accordingly (Wu et al., 2020). There are obvious differences in PM_{2.5} source profiles
187 between SPAPPC (SPAP database and published source profiles in China) and
188 SPECIATE (SPECIATE database), detailed information is shown in Table S3. The
189 percentages of species in PP source profiles are plotted in Fig. 2. The main components
190 in SPAPPC are sorted by Si, SO₄²⁻, OC, Ca with average values of 8.7±6.8%, 8.5±11.5%,
191 6.8±9.1% and 6.5±6.9%, respectively; The SPECIATE are enriched in SO₄²⁻
192 (16.9%±20.0%), OC (12.7±21.8%), Si (9.6±5.0%) and Ca (9.3±7.3%), higher than
193 SPAPPC. Coal properties, burning conditions, pollution control measures and sampling
194 methods are the main reasons for those great percentage fluctuations. Different
195 treatment processes of flue gases, e.g. wet/dry limestone, ammonia and double-alkali
196 flue gas desulfurization, will affect the percentages of components in source profiles
197 (Zhang et al., 2020). It has been reported that the percentage of Ca, Mg, SO₄²⁻ and Cl⁻
198 in PP profiles increased after the limestone-gypsum method was used in coal-fired
199 power plants (Bi et al., 2019). Besides that, the percentage of Cl⁻ in SPAPPC is
200 obviously higher than that in SPECIATE, which might attribute to the generally higher
201 Cl⁻ content in raw coal in China (Guo et al., 2004).



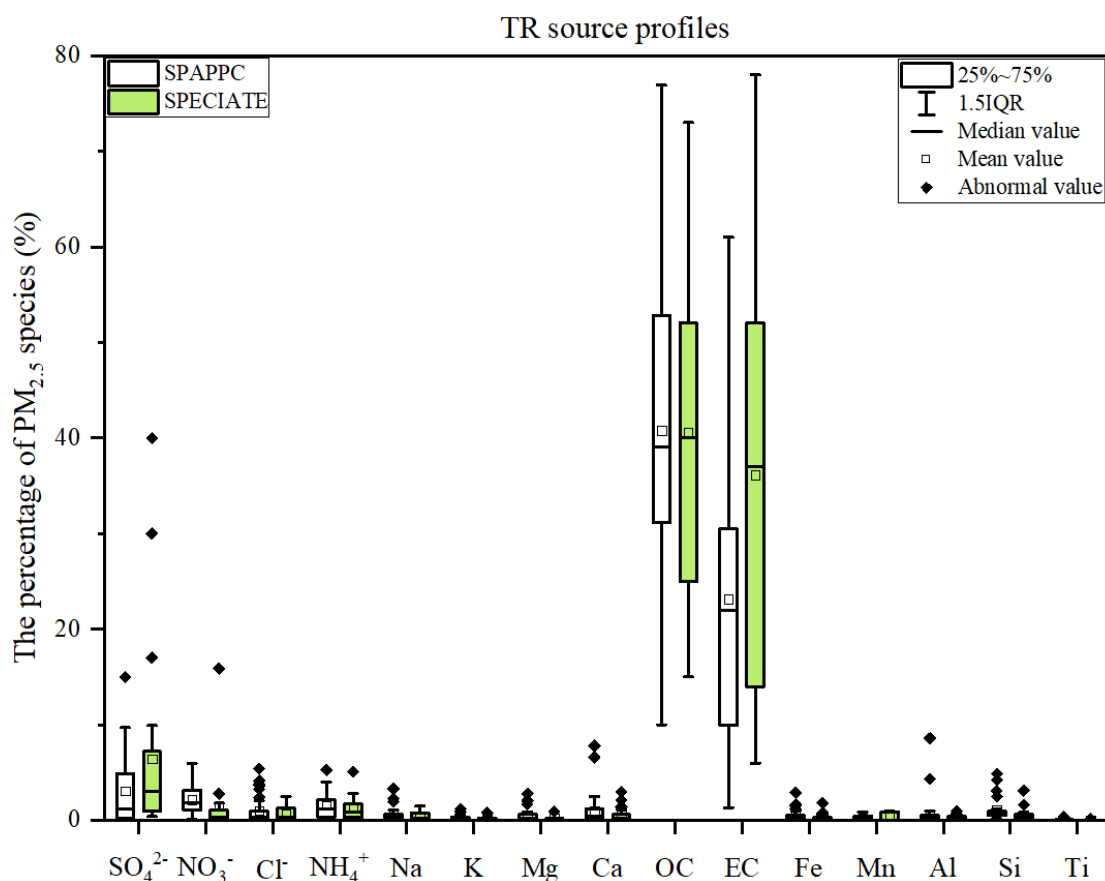
202
 203 Fig. 2 Chemical profiles for $\text{PM}_{2.5}$ emitted from coal-fired power plant (PP). Data obtained from
 204 SPAPPC (SPAP database and published source profiles in China) and SPECIATE (U.S. EPA
 205 SPECIATE database)

206 Industrial emissions are one of the major sources of $\text{PM}_{2.5}$ (Hopke et al., 2020),
 207 the percentages of Ca, Fe, OC and SO_4^{2-} are relatively high both in SPAPPC and
 208 SPECIATE of industrial processes, but the shares in different source profile database
 209 varied (Detailed information were shown in Table S4~S7). In SPAPPC, these four
 210 components account for $16.4 \pm 14.9\%$, $10.4 \pm 14.4\%$, $6.9 \pm 6.1\%$, $6.2 \pm 6.4\%$, the
 211 proportions in SPECIATE are $10.4 \pm 9.8\%$, $11.4 \pm 10.6\%$, $8.5 \pm 4.9\%$, $16.3 \pm 13.3\%$,
 212 respectively (Fig. 3). Large variations of components and their percentages in industrial
 213 processes are attributed to the manufacturing processes, raw material, pollution control
 214 measures and so on (Ji et al., 2017; Bi et al., 2019; Gao et al., 2022). For example, Ca,
 215 Al, OC and SO_4^{2-} are found to have the highest percentage in cement sources (Guo et
 216 al., 2021); Fe, Si and SO_4^{2-} are the most abundant species in steel industry emission
 217 (Guo et al., 2017).



218
219 Fig. 3 Chemical profiles for PM_{2.5} emitted from industry processes (IN). Data obtained from
220 SPAPPC (SPAP database and published source profiles in China) and SPECIATE (U.S. EPA
221 SPECIATE database)

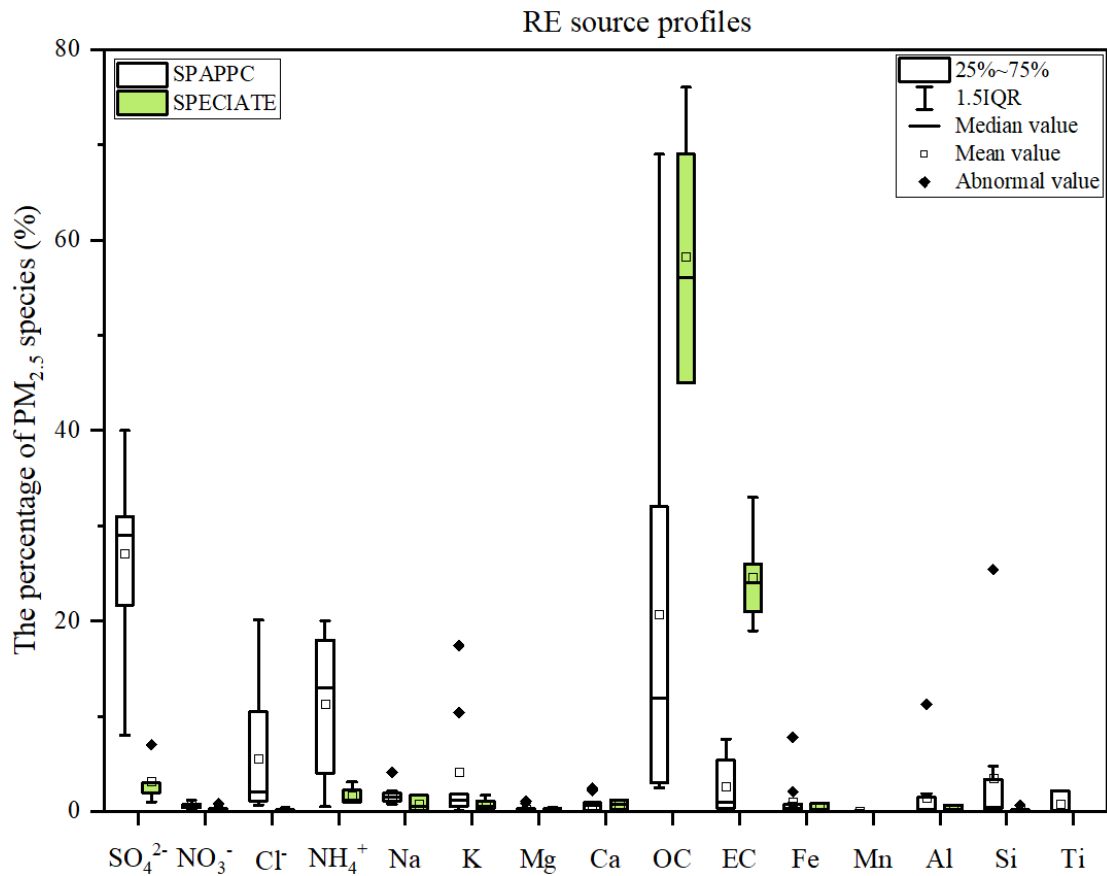
222 Traffic contributed a large fraction of PM_{2.5} in many locations (Hopke et al., 2022).
223 It is well-known that the transportation sector makes a dominant contribution of OC
224 and EC. The main components of PM_{2.5} emitted from traffic sources are OC, EC and
225 SO₄²⁻ both in SPAPPC and SPECIATE, but still vary in wide range (Detailed
226 information was given in Table S8~S10). In SPAPPC, the percentages of OC, EC and
227 SO₄²⁻ are 40.8±15.0%, 23.1±13.8%, 3.1±3.7%, and in SPECIATE, the percentages are
228 40.6±16.4%, 36.1±21.5%, 6.4±9.9%, respectively (Fig. 4). These significant
229 differences mainly attribute to the vehicle type, fuel quality, mixing ratio between oil
230 and gas and the combustion phase in vehicle engine and so on (Xia et al., 2017).



231
 232 Fig. 4 Chemical profiles for $\text{PM}_{2.5}$ emitted from transportation sector (TR). Data obtained from
 233 SPAPPC (SPAP database and published source profiles in China) and SPECIATE (U.S. EPA
 234 SPECIATE database)

235 Residential coal combustion, as the leading source of global $\text{PM}_{2.5}$ emission
 236 (Weagle et al., 2018), has a much higher emission factor than coal-fired power plant
 237 (Wu et al., 2022). The fraction of components varied greatly in the profiles measured
 238 from SPAPPC and SPECIATE (Detailed information was given in Table S11), SO_4^{2-} ,
 239 OC, NH_4^+ and EC make the main contribution to $\text{PM}_{2.5}$ emitted from residential coal
 240 combustion. In SPAPPC, the average percentages of SO_4^{2-} , OC, NH_4^+ , EC are
 241 $27.1 \pm 10.1\%$, $20.7 \pm 20.6\%$, $11.3 \pm 7.7\%$, $2.6 \pm 2.8\%$, respectively. In SPECIATE, the
 242 average percentages are OC ($58.2 \pm 14.0\%$), EC ($24.6 \pm 5.4\%$), SO_4^{2-} ($3.2 \pm 2.3\%$) and
 243 NH_4^+ ($1.6 \pm 1.0\%$) (Fig. 5). Total percentages of OC and EC in SPECIATE are over 80%,
 244 obviously higher than that in SPAPPC, while a higher percentage of SO_4^{2-} , Cl^- , K and
 245 Si are observed in SPAPPC. The coal type and properties, burning condition are the
 246 main factors affecting the percentages of $\text{PM}_{2.5}$ components, like the chunk coal burning
 247 has relatively higher percentages of OC, EC, SO_4^{2-} , NO_3^- and NH_4^+ than honeycomb

248 briquette (Wu et al., 2021; Song et al., 2021).



249
250 Fig. 5 Chemical profiles for PM_{2.5} emitted from residential coal combustion (RE). Data obtained
251 from SPAPPC (SPAP database and published source profiles in China) and SPECIATE (U.S. EPA
252 SPECIATE database)

253 Briefly, many factors can affect PM_{2.5} source profiles, and with the innovation of
254 manufacturing technique and pollution control technology, changes in fuel and raw and
255 auxiliary materials, the main chemical components and their percentages would change
256 dramatically. To explore whether the variations of source profile would be one of the
257 important factors affecting the simulation results of PM_{2.5} species in CTMs, we
258 designed a series of simulation tests as follows.

259 **3 Whether the variation of source profile adopted in CTMs has an impact on the**
260 **simulation of chemical components in PM_{2.5}?**

261 In this part, we separately selected source profiles from SPAPPC and SPECIATE
262 databases and applied them in emission inventory for simulating PM_{2.5} and its
263 components with other modeling conditions unchanged, corresponding to case

264 CMAQ_SPA and CMAQ_SPE. The detailed information of source profiles is shown in
265 Figure S1. To determine the similarity between the two groups of source profiles,
266 Coefficient Divergence (CD) is calculated using the following formula
267 (Wongphatarakul et al., 1998):

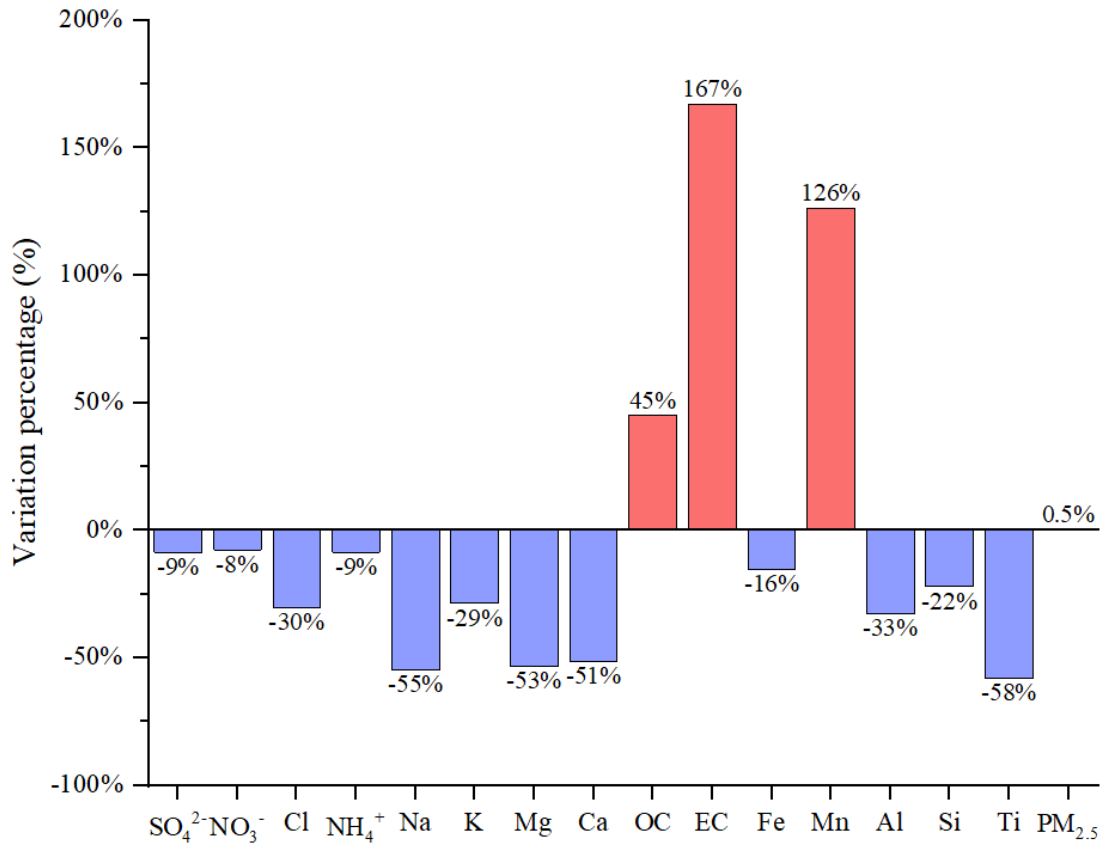
$$268 \quad CD_{jk} = \sqrt{\frac{1}{p} \sum_{i=1}^p \left(\frac{x_{ij} - x_{ik}}{x_{ij} + x_{ik}} \right)^2} \dots\dots\dots (1)$$

269 Where CD_{jk} is the coefficient of divergence of source profile j and k , p was the
270 number of chemical components in source profile, x_{ij} is the weight percentage for
271 chemical component i in source profile j , x_{ik} is the weight percentage for i in source
272 profile k (%). The CD value is in the range of 0 to 1, if the two source profiles are
273 similar, the value of CD is close to 0; if the two are very different, the value was close
274 to 1.

275 By comparing the selected SPAPPC source profiles with the selected SPECIATE
276 source profiles, the coefficient divergences for the four main source categories were
277 $CD_{PP}(0.67) > CD_{RE}(0.62) > CD_{TR}(0.60) > CD_{IN}(0.60)$, which meant the selected source
278 profiles in the two simulation cases were quite different. The simulated concentration
279 of $PM_{2.5}$ and its components (For this part and each test case in next section) at 10
280 ambient air quality monitoring stations (Table S12) were extracted from CMAQ outputs
281 of the innermost simulation domain. We selected one air quality monitoring station to
282 study the influence of $PM_{2.5}$ source profile on numerical simulation of $PM_{2.5}$ -bound
283 components and to explore the relevant laws in the atmosphere, then used the left 9 sites
284 to further illustrate the conclusions suggested.

285 The simulation results for $PM_{2.5}$ species under CMAQ_SPA and CMAQ_SPE
286 cases also showed big differences (as shown in Fig. 6 and Table S13), in which the
287 largest difference in simulated concentration was EC with CAMQ_SPE giving higher
288 by 167% than CMAQ_SPA; For OC and Mn, higher values were also given by
289 CMAQ_SPE than by CMAQ_SPA (45% and 126% on average, respectively); For the
290 remaining components, the simulated concentration by CMAQ_SPE was lower than
291 CMAQ_SPA with Ti (58%), Na (55%), Mg (53%), Ca (51%), Al (33%), Cl (30%), K

292 (29%), Si (22%), Fe (16%), NH₄⁺ (9%), SO₄²⁻ (9%), NO₃⁻ (8%), separately. While the
 293 simulated PM_{2.5} concentrations under the two cases were quite close. The influence of
 294 source profile variation on the simulated PM_{2.5} concentration was not significant, but
 295 the influence on the simulation of chemical components in PM_{2.5} could not be ignored.

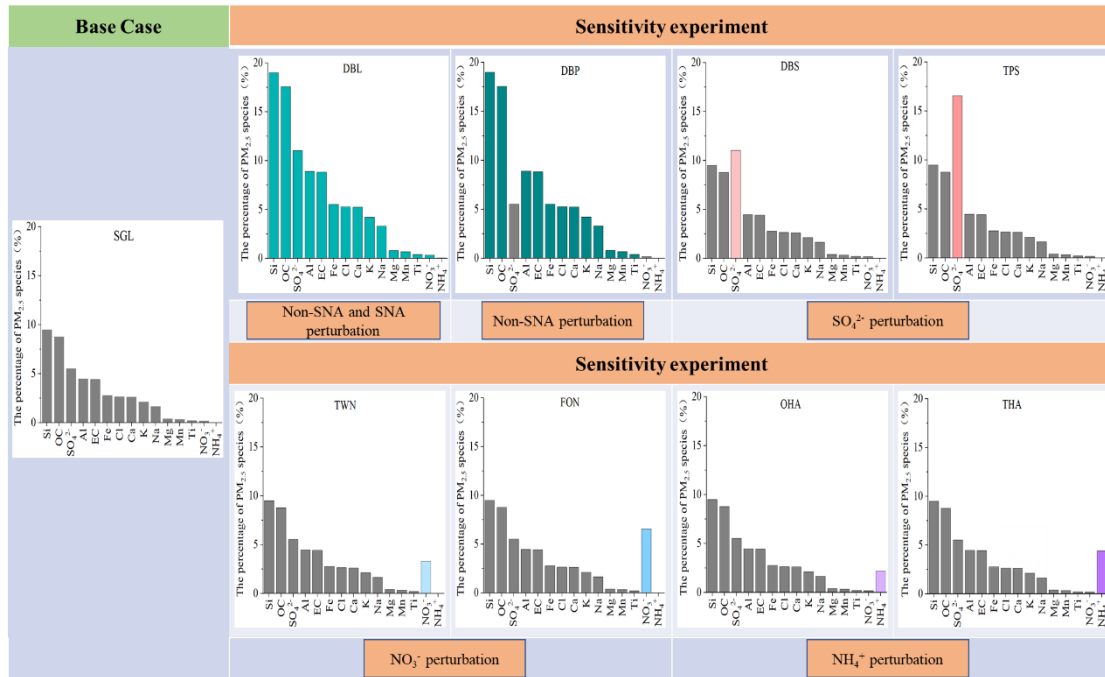


296
 297 Fig. 6 The percentage difference of simulated concentration (PM_{2.5} and its components) between
 298 CMAQ_SPE and CAMQ_SPA (relative to CAMQ_SPA); PM_{2.5} source profiles from SPAPPC and
 299 SPECIATE database were applied in emission inventory for simulating PM_{2.5} and its components,
 300 corresponding to case CMAQ_SPA and CMAQ_SPE, respectively.

301 **4 How much did the variation of source profile adopted in CTMs impact on the**
 302 **simulation of chemical components in PM_{2.5}?**

303 In order to quantitatively characterize how much the source profiles affect the
 304 simulation results of PM_{2.5} and its components, we selected the chemical composition
 305 of code 000002.5 (Variety of different categories, used for the overall average
 306 composite profiles (Hsu et al., 2019)) in the US EPA Speciate_5.0_0 database as species

307 allocation of PM_{2.5} components. The corresponding percentages of EC, OC, Mn, Fe, Ti,
 308 Al, Si, Ca, Mg, K, Na, Cl, NH₄⁺, NO₃⁻ and SO₄²⁻ in PM_{2.5} were shown in Fig. 7 (SGL,
 309 base case simulation).



310
 311 Fig. 7 The general roadmap of sensitivity tests
 312 (The histogram in each case were the speciation profile in CTMs)

313 Table 1 The content of sensitivity experiment cases

Cases	Description
Case S0 (DBL): add perturbation to Non-SNA and SNA	The percentage of all the listed components in the source profile of base case (SGL) were doubled, and the proportion of unlisted components (Other) decreased to 9%.
Case S1 (DBP): add perturbation to Non-SNA	The percentages of non-SNA were doubled and SNA(SO ₄ ²⁻ , NO ₃ ⁻ , NH ₄ ⁺) species stayed the same with that in SGL (the cumulative percentage of listed species was 85.3%), the proportion of unlisted components decreased to 14.7%.
Case S2 (DBS and TPS): add perturbation to SO ₄ ²⁻	The percentage of SO ₄ ²⁻ was doubled (11%, DBS, represented Double Sulfate), tripled (16.5%, TPS, represented Triple Sulfate) and the other listed 14 species stayed the same with that in SGL (the cumulative percentage of listed species was 51% and 57%, respectively), the proportion of unlisted components decreased to 49% and 43%.
Case S3 (TWN and FON): add perturbation to NO ₃ ⁻	The NO ₃ ⁻ content was raised up to 20 times (3.3%, TWN) and 40 times (6.6%, FON) of that in SGL (0.16%), the other 14 species stayed the same with SGL (the cumulative

	percentage of listed species was 48.6% and 51.9%, respectively), the proportion of unlisted components decreased to 51.4% and 48.1%.
Case S4 (OHA and THA): add perturbation to NH_4^+	The NH_4^+ content was raised up to 100 times (2.2%, OHA), 200 times (4.4%, THA) of that in SGL (0.02%), the other 14 species stayed the same with SGL (the cumulative percentage of listed species was 47.7% and 49.9%, respectively), the proportion of unlisted components decreased to 52.3% and 50.1%.

Note: The source profiles in all cases listed in the table were calculated based on the base case SGL. In the design of simulation cases, the reason why the disturbance amplitude of NH_4^+ and NO_3^- were significantly higher than that of other components such as SO_4^{2-} and Non-SNA, was because the percentages of NH_4^+ and NO_3^- in the base source profile (SGL, based on the chemical composition of code 000002.5 in the EPA Speciate_5.0_0 database) were very low, while the percentage of NH_4^+ and NO_3^- in SPAPPC exhibited in section 2.2 were orders of magnitude higher than those in SGL.

314 Given the large number and complex chemical composition of $\text{PM}_{2.5}$, it is
315 advisable to classify it reasonably before designing sensitivity experiments. The Case
316 S0 was to double the percentage of the listed 15 components mentioned above (SGL)
317 in $\text{PM}_{2.5}$ species allocation for emission sources (DBL case, the cumulative percentage
318 was 91%, the details were shown in Fig. 7 and Table 1). As the percentage of these
319 components increased, the proportion of unlisted components (represented by Other)
320 decreased to 9% in order to meet the requirement that the total percentage of all
321 components is 100%. Then we compared the simulation results before (SGL case) and
322 after perturbation (DBL case) in species allocation of $\text{PM}_{2.5}$ sources.

323 In the case DBL, when the percentage of all the components except “other” were
324 doubled in the source profile, the simulated concentrations of Al, Ca, Cl, EC, Fe, K,
325 Mg, Mn, Na, OC, Si and Ti doubled as well, while the simulated concentration of NO_3^- ,
326 SO_4^{2-} and NH_4^+ only increased at about 3%, 10% and 4%, respectively, although the
327 simulated concentration of $\text{PM}_{2.5}$ was not obviously changed (Detailed simulation
328 results were shown in Table S14). Through this Case S0, we found that the results for
329 SNA (SO_4^{2-} , NO_3^- , and NH_4^+) and Non-SNA were obviously different. Therefore, we
330 divided the components in the source profile into two groups (Non-SNA and SNA) and
331 designed a series of sensitivity tests listed in next section to further explore how species

332 allocation of PM_{2.5} in emission sources of CTMs would affect the simulation results.

333 4.1 Sensitivity tests design

334 Based on the Case S0 results, sensitivity tests were designed by changing the
 335 percentages of the target components and related components in the base case (SGL):
 336 perturbation on each component of Non-SNA, perturbation on SO₄²⁻, perturbation on
 337 NO₃⁻, and perturbation on NH₄⁺. The general roadmap of sensitivity tests was shown in
 338 Fig. 7, and the illustration of each case was summarized in Table 1. The basic rules must
 339 be followed: a) perturbation on the percentage of each component in source profile fell
 340 within the variation range of its measured value described in section 2.2. b) The sum of
 341 the percentage of listed Non-SNA, SNA and Other components in PM_{2.5} source profile
 342 was 100%.

343 4.2 Evaluation index for simulation result

344 In order to quantify the concentration changes of simulated PM_{2.5} components
 345 caused by the perturbation in source profile, we proposed the sensitivity coefficient (δ)
 346 as evaluation index. The calculation formula is as follows:

$$\delta_i = \begin{cases} \frac{\frac{C_{i_case}}{C_{PM_{2.5_case}}} \times 100\% - \frac{C_{i_base}}{C_{PM_{2.5_base}}} \times 100\%}{P_{i_case} - P_{i_base}} & \text{(For DBL and DBP)} \\ \frac{\frac{C_{i_case}}{C_{PM_{2.5_case}}} \times 100\% - \frac{C_{i_base}}{C_{PM_{2.5_base}}} \times 100\%}{P_{j_case} - P_{j_base}} & \text{(For other cases)} \end{cases} \dots\dots\dots (2)$$

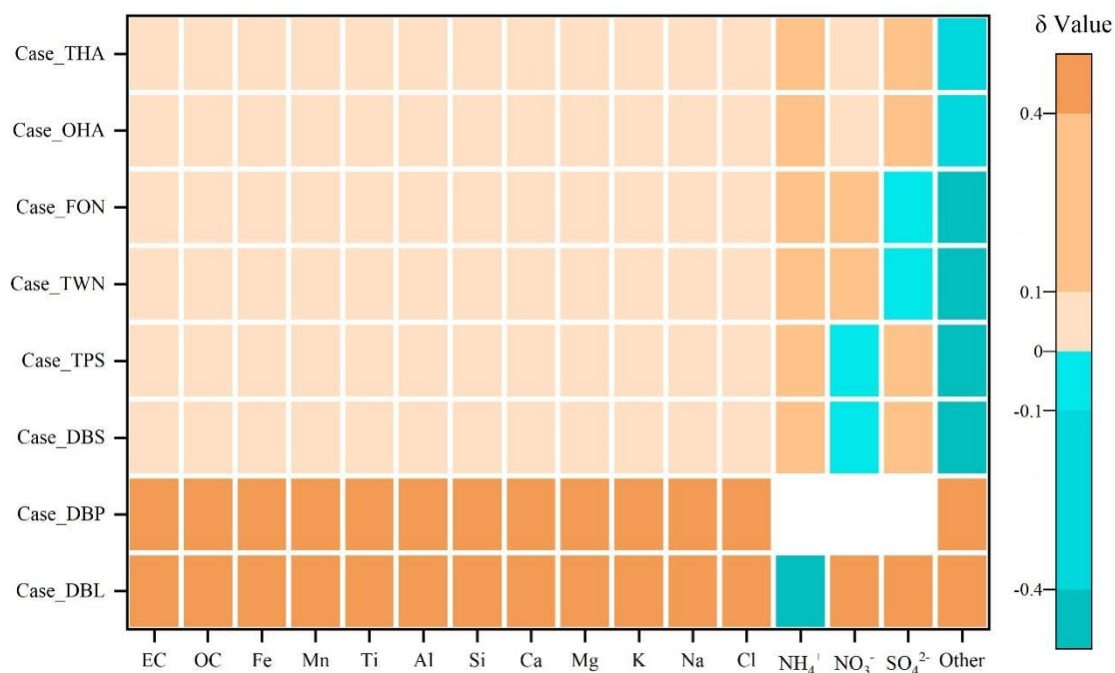
348 Wherein, δ_{*i*} is the sensitivity coefficient of component *i*, representing the change
 349 of the simulated value of its content in ambient PM_{2.5} corresponded to 1% perturbation
 350 in the source profiles. C_{*i*_case} is the simulation result of component *i* in different
 351 sensitivity experiment cases, µg/m³; C_{*i*_base} is the simulation result of components *i* in
 352 base case, µg/m³; C_{PM_{2.5}_case} is the simulation result of PM_{2.5} in different sensitivity
 353 experiment cases, µg/m³; C_{PM_{2.5}_base} is the simulation result of PM_{2.5} in base case, µg/m³;
 354 P_{*i*_case} is the percentage of component *i* in different source profile of sensitivity
 355 experiment cases, %; P_{*j*_case} is the percentage of perturbed component *j* in different

356 source profile of sensitivity experiment cases, %; P_{i_base} is the percentage of component
357 i in base case source profile, %; ; P_{j_base} is the percentage of perturbed component j in
358 base case source profile, %.

359 The positive value of δ means the simulated concentration of PM_{2.5} component
360 increases (decreases) with the increase (decrease) of the perturbation to the percentage
361 of components in source profile, while the meaning of negative δ is just the opposite. If
362 the absolute value of δ is less than or equal to 0.1, the simulated result of PM_{2.5} chemical
363 component is considered to be insensitive to the corresponding variation of source
364 profile; If the absolute value of δ falls between 0.1 and 0.4 (included), the simulated
365 results of PM_{2.5} chemical component is considered to be sensitive to the variation of
366 source profile; If the absolute value of δ is larger than 0.4, the simulated results of PM_{2.5}
367 chemical component is very sensitive to the variation of source profile. The greater the
368 absolute value of δ is, indicates the variation of source profile adopted in CMAQ has
369 more obvious impact on the simulated results of PM_{2.5} chemical components.

370 **4.3 The response of simulated PM_{2.5} components**

371 Fig.8 listed the sensitivity coefficients of simulated ambient PM_{2.5} components to
372 the perturbation of source profile under each test case. In case DBL (The percentage of
373 all the listed components in the source profile of base case (SGL) was doubled), the
374 sensitivity coefficient (δ) of NH₄⁺ was negative, and the absolute value was the highest,
375 indicating that the simulated proportion of NH₄⁺ in ambient PM_{2.5} decreased, and it was
376 very sensitive to the variation of source profile. Conversely, the sensitivity coefficient
377 of NO₃⁻ was close to 1, which illustrated that the simulated proportion of NO₃⁻ in
378 ambient PM_{2.5} increased proportionally with the change in source profile. The δ of SO₄²⁻
379 also showed a very sensitive property. The simulated Non-SNA concentrations were
380 doubled when compared to the base case (SGL).



381
 382 Fig. 8 The sensitivity coefficients (δ) of simulated components to the perturbation of adopted source
 383 profile in different cases. Note: Each small color box in the figure represented the sensitivity level
 384 (indicated by the legend on the right) of $PM_{2.5}$ components (the x-coordinate) in different cases (y-
 385 coordinate). The blank grids in DBP case indicated no perturbation to SNA in $PM_{2.5}$ source profile
 386 under this case.

387 In case DBP, when the percentages of listed Non-SNA in the source profile were
 388 doubled, the simulated proportions of Non-SNA (Al, Ca, Cl, EC, Fe, K, Mg, Mn, Na,
 389 OC, Si and Ti) in ambient $PM_{2.5}$ synchronous increased, and were very sensitive to the
 390 change in the adopted source profile with a sensitivity coefficient (δ) of 0.5.
 391 Interestingly, the simulated concentration of SNA in ambient $PM_{2.5}$ also changed
 392 although the SNA in source profile did not change, the concentration of NO_3^- and SO_4^{2-}
 393 increased by 2% and 3%, respectively, NH_4^+ decreased by 10% (Detail simulation
 394 results of different cases were shown on Table S15~S21).

395 Under SO_4^{2-} perturbation cases (Case DBS and Case TPS), we found the simulated
 396 results of Non-SNA and NO_3^- had no obvious variation when compared with the base
 397 case. Either in Case DBS or in Case TPS, the δ of Non-SNA and NO_3^- were always
 398 between -0.1 to 0.1. But when the percentage of SO_4^{2-} was doubled in $PM_{2.5}$ source
 399 profile (DBS), the simulated concentration of NH_4^+ and SO_4^{2-} increased by 6% and 8%,
 400 respectively. In Case TPS (the percentage of SO_4^{2-} was tripled), the simulated

401 concentration of NH_4^+ and SO_4^{2-} were increased by 11% and 16%, respectively. The δ
402 of NH_4^+ and SO_4^{2-} were 0.12 and 0.36, sensitive toward to positive direction with the
403 increase of SO_4^{2-} in the source profile.

404 In the situation of NO_3^- perturbation (Case TWN and Case FON), the simulated
405 concentrations of Non-SNA hardly change when compared to the base case, while the
406 changing characteristics of SNA concentrations were different. In cases TWN and FON,
407 the simulation concentration of NH_4^+ increased by 2.6% and 5.4% when compared with
408 the base case, the simulated NO_3^- increased by 14% and 30%, the simulated SO_4^{2-}
409 decreased slightly, even could be neglected in some observation sites. The simulated
410 concentrations of Non-SNA and SO_4^{2-} were insensitive to the perturbation of NO_3^- in
411 $\text{PM}_{2.5}$ source profile; NH_4^+ was sensitive, and NO_3^- was very sensitive.

412 When we put perturbation to NH_4^+ in the source profile (Case OHA and Case
413 THA), the simulation results of Non-SNA were almost not changed, the simulated
414 concentration of SO_4^{2-} , NH_4^+ , NO_3^- increased in OHA and THA. The δ of SNA to the
415 variation of NH_4^+ in the source profile were positive and $\delta(\text{SO}_4^{2-}) > \delta(\text{NH}_4^+) > \delta(\text{NO}_3^-)$,
416 SO_4^{2-} and NH_4^+ were sensitive to the NH_4^+ perturbation in the source profile, but NO_3^-
417 was not so sensitive.

418 In general, the simulation results of components in ambient $\text{PM}_{2.5}$ were affected in
419 one way or another by the change of source profiles adopted by CMAQ. Both of the
420 simulated Non-SNA and SNA were very sensitive to the perturbation of Non-SNA in
421 source profile. When the percentage of SNA changed in the source profile, simulated
422 concentrations of Non-SNA generally have little change, but the simulation results of
423 SNA could change in different levels: the simulated SO_4^{2-} was very sensitive and NH_4^+
424 was sensitive to the perturbation of SO_4^{2-} in source profile, simulated NO_3^- was very
425 sensitive and NH_4^+ was sensitive to the perturbation of NO_3^- , SO_4^{2-} and NH_4^+ were
426 sensitive to the perturbation of NH_4^+ . The simulated component such as SO_4^{2-} was
427 influenced not only by the change of SO_4^{2-} itself but also by other components like
428 some Non-SNA and NH_4^+ in the source profile. In other words, there was a linkage
429 effect, variation of some components in the source profile would bring changes to the

430 simulated results of other components.

431 **5 How the variation of source profile adopted in CTMs impact on the simulation**
432 **of chemical components in PM_{2.5}?**

433 The variation of species allocation in emission sources directly affected the
434 composition of aerosol system in CTMs. In CMAQv5.0.2, the aerosol thermodynamic
435 equilibrium process was carried out according to ISORROPIA II, including a SO₄²⁻-
436 NO₃⁻-Cl⁻-NH₄⁺-Na⁺-K⁺-Mg²⁺-Ca²⁺-H₂O system which was established on the basis of
437 ISORROPIA I by adding the effects of K⁺, Ca²⁺ and Mg²⁺ (Detailed equilibrium
438 relations were shown in Table S22). Some assumptions had been made in the
439 ISORROPIA model to simplify the simulation system (Fountoukis and Nenes, 2007):
440 (1) Because the vapor pressure of sulfuric acid and metal salts (such as Na⁺, Ca²⁺, K⁺,
441 Mg²⁺) were very low, it was assumed that all the sulfuric acid and metal salts in the
442 system existed in the aerosol phase; (2) For ammonia in the system, it was preferred to
443 have an irreversible reaction with sulfuric acid to produce ammonium sulfate. Only
444 when there was still surplus NH₃ after the neutralization of H₂SO₄, can it have a
445 reversible reaction with HNO₃ and HCl to produce NH₄NO₃ and NH₄Cl. (3) For sulfuric
446 acid in the system, if there were metal ions (such as Ca²⁺, Mg²⁺, K⁺, Na⁺) in the system,
447 sulfuric acid would react with metal ions to produce metal salts. Only in the case of
448 insufficient sodium, sulfuric acid would react with ammonia. Based on these
449 assumptions, the ISORROPIA model introduced the following three judgment
450 parameters (R₁, R₂ and R₃ were calculated by the following formulas) to determine the
451 simulation subsystems. In this paper, R₁, R₂, R₃ and the corresponding solid phase
452 species under different perturbation cases on source profiles were shown in Table 3.
453 These components achieved thermodynamic equilibrium in the order of preference for
454 more stable salts, obviously, the simulation processes of these components may
455 influence each other.

456
$$R_1 = \frac{[\text{NH}_4^+] + [\text{Ca}^{2+}] + [\text{K}^+] + [\text{Mg}^{2+}] + [\text{Na}^+]}{[\text{SO}_4^{2-}]} \dots\dots\dots (3)$$

457
$$R_2 = \frac{[Ca^{2+}] + [K^+] + [Mg^{2+}] + [Na^+]}{[SO_4^{2-}]} \dots\dots\dots (4)$$

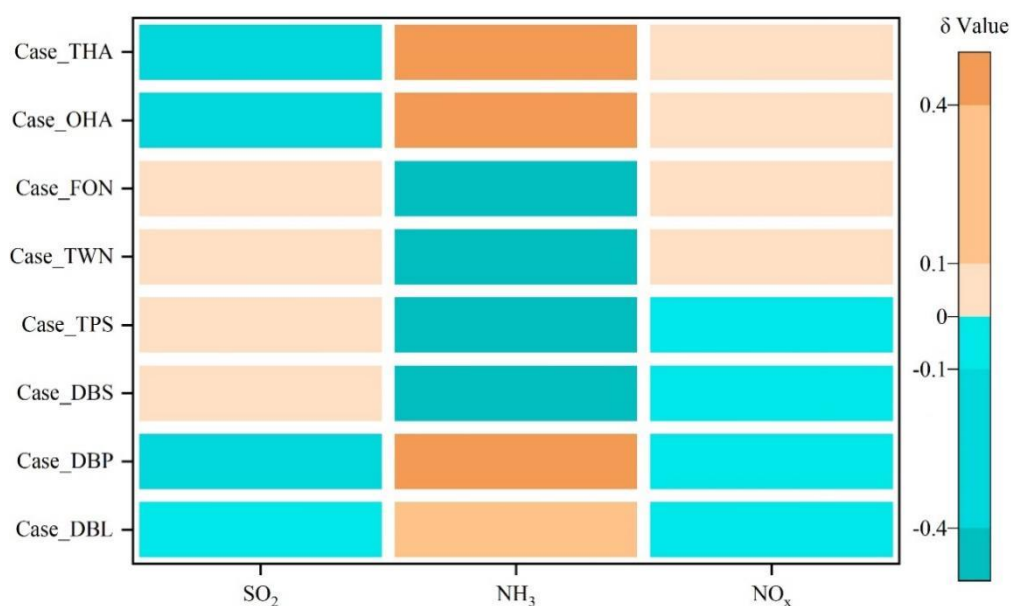
458
$$R_3 = \frac{[Ca^{2+}] + [K^+] + [Mg^{2+}]}{[SO_4^{2-}]} \dots\dots\dots (5)$$

459 Table 2 Potential aerosol species in ISORROPIA II under different cases

Cases	R ₁	R ₂	R ₃	Solid phase species*
SGL、DBL TWN、FON	2.53	2.52	1.9	CaSO ₄ , MgSO ₄ , K ₂ SO ₄ , Na ₂ SO ₄ , NaCl, NaNO ₃ , NH ₄ Cl, NH ₄ NO ₃
DBS	1.26	1.26	0.95	CaSO ₄ , MgSO ₄ , K ₂ SO ₄ , KHSO ₄ , Na ₂ SO ₄ , NaHSO ₄ , (NH ₄) ₂ SO ₄ , NH ₄ HSO ₄ , (NH ₄) ₃ H(SO ₄) ₂
TPS	0.84	0.84	0.63	CaSO ₄ , KHSO ₄ , NaHSO ₄ , NH ₄ HSO ₄
DBP	5.04	5.03	3.79	CaSO ₄ , MgSO ₄ , K ₂ SO ₄ , CaCl ₂ , Ca(NO ₃) ₂ , MgCl ₂ ,
OHA	3.58	2.52	2.95	Mg(NO ₃) ₂ , KCl, KNO ₃ , NaCl, NaNO ₃ , NH ₄ Cl,
THA	4.64	2.52	4.02	NH ₄ NO ₃

460 * The solid phase species were determined based on the research of (Fountoukis and Nenes, 2007)

461 In Non-SNA perturbation case, when the percentage of Non-SNA in source profile
 462 doubled (Case DBP), meant there were more Na, K, Mg, Ca, Cl participated in aerosol
 463 chemistry, the model system needed more SO₄²⁻ and NO₃⁻ on the basis of charge balance
 464 and the thermodynamic equilibrium shifted to the direction of consuming Ca Mg, K
 465 and Na, which resulted in the increase of the simulated concentration of SO₄²⁻ and NO₃⁻.
 466 Meanwhile, according to the rule of anions preferentially binding with nonvolatile
 467 cations in ISORROPIA, the increased cations Na⁺, K⁺, Mg²⁺, Ca²⁺ directly led to
 468 the decrease of anions binding with NH₄⁺, there were less reaction dose between SO₄²⁻
 469 and NH₄⁺ to form (NH₄)₂SO₄ or NH₄HSO₄, ultimately resulted in a decrease in
 470 simulated concentration of NH₄⁺ when compared to the base case. Because in this case
 471 more anions such as SO₄²⁻ were passively needed, according to the principle of chemical
 472 equilibrium mentioned above, the chemical conversion of SO₂ to SO₄²⁻ was promoted,
 473 the simulated secondary SO₄²⁻ increased, this could be proved by that the δ of SO₂ in
 474 Case DBP was negative (shown in Fig. 9, details of other monitoring stations were
 475 shown Table S24).



476
477 Fig.9 The sensitivity coefficients (δ) of simulated gas pollutants to the change of adopted source
478 profile in different cases.

479 Similarly, with the increase of metal ions in the system to bond with anions, the
480 number of anions which can bind to NH_4^+ decreased. The system needed less NH_4^+ and
481 weakened the need for conversion from NH_3 to NH_4^+ , the simulated NH_4^+ concentration
482 decreased while the δ of NH_3 was positive and very sensitive. Different trends of
483 simulated concentration of gaseous pollutants mirrored the rules mentioned above from
484 another aspect. The δ of SO_2 and NO_x was negative, NH_3 was positive. We could see
485 the same phenomena in DBL case (Fig. 9). When the percentages of Non-SNA in source
486 profile increased, they not only affected the simulated concentration of Non-SNA, but
487 also the secondary SO_4^{2-} , NO_3^- and NH_4^+ .

488 In SO_4^{2-} perturbation cases (Case DBS and TPS), as the percentage of SO_4^{2-} in
489 source profile increased, for the chemical reactions of sulfate radical consuming (as
490 shown in Table S22), the chemical equilibrium would move toward the products when
491 compared to the base case. While for the chemical reactions of sulfate radical formation
492 (The equations were shown in Table S23), meant the product was added in, the chemical
493 equilibrium would be pushed toward the reactants. The chemical reactions between
494 SO_4^{2-} and NH_4^+ would shift to the direction of $(\text{NH}_4)_2\text{SO}_4$ generation, we could see the
495 simulated concentrations of NH_4^+ in DBS and TPS were both higher and NH_3 were
496 lower than those in the base case (SGL). In addition, when more SO_4^{2-} was added in,

497 the conversion of SO_2 to SO_4^{2-} was affected in some level and consumed less SO_2 than
498 the base case, simulated SO_2 showed insensitive but positive trend (Fig.9). And from
499 the potential solid phase species in ISORROPIA II under DBS and TPS cases (Table 3),
500 the solid phase species were mainly consisted of sulfate salts, so the simulated
501 concentration of NO_3^- did not change apparently.

502 As the percentage of NO_3^- in source profile increased (Case FON and TWN), the
503 associated chemical equilibrium shifted towards the consumption of NO_3^- , such as NH_4^+
504 $+ \text{NO}_3^- \rightarrow \text{NH}_4\text{NO}_3$, which would also consume more NH_4^+ and form more ammonium
505 salt, finally consumed more NH_3 because of $\text{NH}_3(\text{gas}) + \text{H}_2\text{O}(\text{aq}) \rightarrow \text{NH}_4^+(\text{aq}) + \text{OH}^-$
506 (aq). The simulation results also manifested that the concentration of NH_4^+ increased
507 while that of NH_3 decreased. Based on the assumption of ISORROPIA, the cations like
508 Na^+ , K^+ , Mg^{2+} , Ca^{2+} and NH_4^+ preferentially to react with SO_4^{2-} , only if there were
509 cations left after neutralized SO_4^{2-} , could they react with NO_3^- to form salts, so the
510 simulated concentration of SO_4^{2-} was not obviously changed. Accordingly, the
511 simulated concentration of NO_x and SO_2 almost unchanged (The δ of NO_x and SO_2 was
512 insensitive).

513 In the cases of NH_4^+ perturbation (Case OHA and THA), when the percentage of
514 NH_4^+ in source profile increased, the related chemical equilibrium shifted towards the
515 direction of NH_4^+ consumption, such as in $2\text{NH}_4^+ + \text{SO}_4^{2-} \rightarrow (\text{NH}_4)_2\text{SO}_4$, more SO_4^{2-}
516 was consumed at the same time, which further promoted the conversion of SO_2 to SO_4^{2-} .
517 The increased NH_4^+ in OHA and THA also would inhibit the conversion of NH_3 to NH_4^+
518 when compared to the base case. This, in turn appeared as the increase of the simulated
519 secondary SO_4^{2-} and NH_3 , and the decrease of the simulated SO_2 .

520 In summary, the effects of source profile variation on the simulation results of
521 different components were linked. When the percentages of Non-SNA, SO_4^{2-} , NO_3^- and
522 NH_4^+ in the source profile changed, they not only affected the simulated concentration
523 of themselves, but also affected the simulation results of some other components. Both
524 the simulation results of primary components and secondary components were affected
525 by the change of source profile, the secondary SO_4^{2-} and NH_4^+ were affected more than

526 the secondary NO_3^- .

527 **6 Conclusions**

528 Although the influence of source profile variation on the simulated concentration
529 of ambient $\text{PM}_{2.5}$ is not significant, its influence on the simulated chemical components
530 cannot be ignored. The variation of simulated components ranges from 8% to 167%
531 under selected different source profiles, and the simulation results of some components
532 are sensitive to the adopted $\text{PM}_{2.5}$ source profile in CTMs, e.g., both the simulated Non-
533 SNA and SNA are sensitive to the perturbation of Non-SNA in source profile, the
534 simulated SO_4^{2-} and NH_4^+ are sensitive to the perturbation of SO_4^{2-} , simulated NO_3^- and
535 NH_4^+ are sensitive to the perturbation of NO_3^- , SO_4^{2-} and NH_4^+ are sensitive to the
536 perturbation of NH_4^+ . These influences are not only specific to an individual component,
537 but also can be transmitted and linked among components, that is, the influence path is
538 connected to chemical mechanisms in the model since the variation of species allocation
539 in emission sources directly affect the thermodynamic equilibrium system
540 (ISORROPIA II, SO_4^{2-} - NO_3^- - Cl^- - NH_4^+ - Na^+ - K^+ - Mg^{2+} - Ca^{2+} - H_2O system).

541 Traditionally, the source profiles are regarded as a primary emission, but
542 interestingly, their variation could affect the simulation result of secondary components
543 as well in CTMs. We found the perturbation of $\text{PM}_{2.5}$ source profile caused the variation
544 of simulated gaseous pollutants, and related chemical reactions like gas-phase
545 chemistry of SO_2 , NO_x and NH_3 , which mirrored that the perturbation of source profile
546 had an effect on the simulation of secondary $\text{PM}_{2.5}$ components. Overall, the emission
547 source profile used in CTMs is one of the important factors affecting the simulation
548 results of $\text{PM}_{2.5}$ chemical components. Additionally, organic species are one of the most
549 important components in $\text{PM}_{2.5}$ and gain much more attention on human health. While
550 the number of organic species in source profile is relatively scarce which brings a
551 challenge for simulation test designing, the variation of source profile adopted in CTMs
552 has an impact on the simulation of organic species is not taken into account in this study.

553 With the change of fuel and raw materials, the development of production

554 technology and the innovation of pollution treatment technology in recent years, some
555 components have changed significantly in the source profile. Given the important role
556 of air quality simulation in environment management and health risk assessment, the
557 representativeness and timeliness of the source profile should be considered.

558 Our study tentatively discussed the impact mechanism of emission source profiles
559 on PM_{2.5} components simulation results in CTMs. In the next work, we will use
560 different source profile for simulation, compare the simulation results with local
561 measured PM_{2.5} components and discuss the influence of sub-source profiles variation
562 on the simulation results. In addition, the size distribution, mixing state, aging and
563 solubility for different aerosol components might have something to do with source
564 profile, how much the influence of source profile changes on these physical and
565 chemical process, is deserved to do in the future.

566 **Data availability**

567 The input datasets for WRF simulation are available at
568 <https://rda.ucar.edu/datasets/ds351.0/index.html> (The National Center for Atmospheric
569 Research (NCAR)). The Multi-resolution Emission Inventory for China (MEICv1.3) is
570 available at http://meicmodel.org/?page_id=135. The PM_{2.5} emission source profiles
571 from database of Source Profiles of Air Pollution (SPAP)
572 (<http://www.nkspap.com:9091/>, Nankai university), SPECIATE database
573 (<https://www.epa.gov/air-emissions-modeling/speciate>, U.S. Environmental Protection
574 Agency's (EPA)), Mendeley data repository (<https://doi.org/10.17632/x8dfshjt9j.2>, Bi
575 et al., 2019).

576 **Code availability**

577 The source code for CMAQ version 5.0.2 is available at
578 <https://github.com/USEPA/CMAQ/tree/5.0.2> (last access: April 2014)
579 (<https://doi.org/10.5281/zenodo.1079898>, US EPA Office of Research and
580 Development, 2018). The source code for WRF version 3.7.1 is available at
581 <https://www2.mmm.ucar.edu/wrf/src/WRFV3.7.1.TAR.gz>.

582 **Author contributions**

583 Zhongwei Luo: Data curation and collection, writing–original draft. Yan Han:
584 Modeling, writing–original draft. Kun Hua: Data collection. Yufen Zhang:
585 Supervision–Review & editing. Jianhui Wu: Supervision in source profile. Xiaohui Bi:
586 Supervision in source profile. Qili Dai: Resources. Baoshuang Liu: Resources. Yang
587 Chen: Modification and editing. Xin Long: Supervision in modeling. Yinchang Feng:
588 Supervision–Review & editing.

589 **Competing interests**

590 The authors declare that they have no known competing financial interests or
591 personal relationships that could have appeared to influence the work reported in this
592 paper.

593 **Disclaimer. Publisher’s note**

594 Copernicus Publications remains neutral with regard to jurisdictional claims in
595 published maps and institutional affiliations.

596 **Acknowledgements**

597 We would like to thank the National Natural Science Foundation of China (grant
598 number 42177465) for providing funding for the project. We are grateful for the
599 Inventory Spatial Allocate Tool (ISAT) provided by Kun Wang from Department of Air
600 Pollution Control, Institute of Urban Safety and Environmental Science, Beijing
601 Academy of Science and Technology. We thank two anonymous referees and Astrid
602 Kerkweg (Executive Editor) for helpful discussion.

603 **Financial support**

604 This study was financially supported by the National Natural Science Foundation
605 of China (grant number 42177465).

606 **Reference**

607 Appel, K. W., Poullo, G. A., Simon, H., Sarwar, G., Pye, H. O. T., Napelenok, S. L., Akhtar, F., Roselle,

608 S. J.: Evaluation of dust and trace metal estimates from the Community Multiscale Air Quality
609 (CMAQ) model version 5.0, *Geosci. Model Dev.*, 6, 883-899, [https://doi.org/10.5194/gmd-6-883-](https://doi.org/10.5194/gmd-6-883-2013)
610 2013, 2013.

611 Bi, X., Dai, Q., Wu, J., Zhang, Q., Zhang, W., Luo, R., Cheng, Y., Zhang, J., Wang, L., Yu, Z., Zhang, Y.,
612 Tian, Y., Feng, Y.: Characteristics of the main primary source profiles of particulate matter across
613 China from 1987 to 2017, *Atmos. Chem. Phys.*, 19, 3223-3243, [https://doi.org/10.5194/acp-19-](https://doi.org/10.5194/acp-19-3223-2019)
614 3223-2019, 2019.

615 Cao, J., Qiu, X., Gao, J., Wang, F., Wang, J., Wu, J., Peng, L.: Significant decrease in SO₂ emission and
616 enhanced atmospheric oxidation trigger changes in sulfate formation pathways in China during
617 2008–2016, *J. Clean. Prod.*, 326, 129396, <https://doi.org/10.1016/j.jclepro.2021.129396>, 2021.

618 Chapel Hill, N.: Operational Guidance for the Community Multiscale Air Quality (CMAQ) Mo
619 deling System Version 5.0, [https://www.airqualitymodeling.org/index.php/CMAQ_version_5.0_](https://www.airqualitymodeling.org/index.php/CMAQ_version_5.0_(February_2010_release)_OGD#Aerosol_Module)
620 (February_2010_release)_OGD#Aerosol_Module, last access: February 2012.

621 Chen, Z., Chen, D., Zhao, C., Kwan, M., Cai, J., Zhuang, Y., Zhao, B., Wang, X., Chen, B., Yang, J., Li,
622 R., He, B., Gao, B., Wang, K., Xu, B.: Influence of meteorological conditions on PM_{2.5}
623 concentrations across China: A review of methodology and mechanism, *Environ. Int.*, 139, 105558,
624 <https://doi.org/10.1016/j.envint.2020.105558>, 2020.

625 Cheng, N. L., Meng, F., Wang, J. K., Chen, Y. B., Wei, X., Han, H.: Numerical simulation of the spatial
626 distribution and deposition of PM_{2.5} in East China coastal area in 2010 (In Chinese), *Journ. Safety*
627 *Environ.*, 15, 305-310, <https://doi.org/10.13637/j.issn.1009-6094.2015.06.063>, 2015.

628 Foley, K. M., Roselle, S. J., Appel, K. W., Bhave, P. V., Pleim, J., Otte, T., Mathur, R., Sarwar, G., Young,
629 J. O., Gilliam, R.: Incremental testing of the community multiscale air quality (CMAQ) modeling
630 system version 4.7, *Geosci. Model Dev.*, 3, 205-226, <https://doi.org/10.5194/gmd-3-205-2010>, 2010.

631 Fountoukis, C., Nenes, A.: ISORROPIA II: a computationally efficient thermodynamic equilibrium
632 model for K⁺–Ca²⁺–Mg²⁺–NH₄⁺–Na⁺–SO₄²⁻–NO₃⁻–Cl⁻–H₂O aerosols, *Atmos. Chem. Phys.*, 7,
633 4639-4659, <https://doi.org/10.5194/acp-7-4639-2007>, 2007.

634 Fu, X., Wang, S., Zhao, B., Xing, J., Cheng, Z., Liu, H., Hao, J.: Emission inventory of primary pollutants
635 and chemical speciation in 2010 for the Yangtze River Delta region, China, *Atmos. Environ.*, 70,
636 39-50, <https://doi.org/10.1016/j.atmosenv.2012.12.034>, 2013.

637 Fu, X., Wang, S. X., Chang, X., Cai, S., Xing, J., Hao, J. M.: Modeling analysis of secondary inorganic
638 aerosols over China: pollution characteristics, and meteorological and dust impacts, *Sci. Rep.*, 6,
639 35992, <https://doi.org/10.1038/srep35992>, 2016.

640 Gao, S., Zhang, S., Che, X., Ma, Y., Chen, X., Duan, Y., Fu, Q., Wang, S., Zhou, B., Wei, C., Jiao, Z.:
641 New understanding of source profiles: Example of the coating industry, *J. Clean. Prod.*, 357, 132025,
642 <https://doi.org/10.1016/j.jclepro.2022.132025>, 2022.

643 Guo, R., Yang, J., Liu, Z.: Influence of heat treatment conditions on release of chlorine from Datong coal,
644 *J. Anal. Appl. Pyrol.*, 71, 179-186, [https://doi.org/10.1016/S0165-2370\(03\)00086-X](https://doi.org/10.1016/S0165-2370(03)00086-X), 2004.

645 Guo, Y. Y., Gao, X., Zhu, T. Y., Luo, L., Zheng, Y.: Chemical profiles of PM emitted from the iron and
646 steel industry in northern China, *Atmos. Environ.*, 150, 187-197,
647 <https://doi.org/10.1016/j.atmosenv.2016.11.055>, 2017.

648 Guo, Z., Hao, Y., Tian, H., Bai, X., Wu, B., Liu, S., Luo, L., Liu, W., Zhao, S., Lin, S., Lv, Y., Yang, J.,
649 Xiao, Y.: Field measurements on emission characteristics, chemical profiles, and emission factors
650 of size-segregated PM from cement plants in China, *Sci. Total Environ.*, 151822,
651 <https://doi.org/10.1016/j.scitotenv.2021.151822>, 2021.

652 Han, Y., Xu, H., Bi, X. H., Lin, F. M., Li, J., Zhang, Y. F., Feng, Y. C.: The effect of atmospheric
653 particulates on the rainwater chemistry in the Yangtze River Delta, China, *J. Air Waste Manage.*, 69,
654 1452-1466, <https://doi.org/10.1080/10962247.2019.1674750>, 2019.

655 Hopke, P. K., Dai, Q., Li, L., Feng, Y.: Global review of recent source apportionments for airborne
656 particulate matter, *Sci. Total Environ.*, 740, 140091,
657 <https://doi.org/10.1016/j.scitotenv.2020.140091>, 2020.

658 Hopke, P. K., Feng, Y. C., Dai, Q.: Source apportionment of particle number concentrations: A global
659 review, *Sci. Total Environ.*, 819, 153104, <https://doi.org/10.1016/j.scitotenv.2022.153104>, 2022.

660 Hsu, Y., Divita, F., Dorn, J.: SPECIATE 5.0 - Speciation Database Development Documentation, Final
661 Report, M. MENETREZ, Abt Associates Inc./Office of Research and Development/U.S.
662 Environmental Protection Agency Research Triangle Park, NC27711,
663 https://www.epa.gov/sites/default/files/2019-07/documents/speciate_5.0.pdf, 2019.

664 Huang, C. H., Hu, J. L., Xue, T., Xu, H., Wang, M.: High-Resolution Spatiotemporal Modeling for
665 Ambient PM_{2.5} Exposure Assessment in China from 2013 to 2019, *Environ. Sci. Technol.*, 55, 2152-
666 2162, <https://doi.org/10.1021/acs.est.0c05815>, 2021.

667 Huang, Z. J., Zheng, J. Y., Qu, J. M., Zhong, Z. M., Wu, Y. Q., Shao, M.: A Feasible Methodological
668 Framework for Uncertainty Analysis and Diagnosis of Atmospheric Chemical Transport Models,
669 *Environ. Sci. Technol.*, 53, 3110-3118, <https://doi.org/10.1021/acs.est.8b06326>, 2019.

670 Ji, Z., Gan, M., Fan, X., Chen, X., Li, Q., Lv, W., Tian, Y., Zhou, Y., Jiang, T.: Characteristics of PM_{2.5}
671 from iron ore sintering process: Influences of raw materials and controlling methods, *J. Clean. Prod.*,
672 148, 12-22, <https://doi.org/10.1016/j.jclepro.2017.01.103>, 2017.

673 Li, J., Wu, Y., Ren, L., Wang, W., Tao, J., Gao, Y., Li, G., Yang, X., Han, Z., Zhang, R.: Variation in PM_{2.5}
674 sources in central North China Plain during 2017–2019: Response to mitigation strategies, *J.*
675 *Environ. Manage.*, 28, 112370, <https://doi.org/10.1016/j.jenvman.2021.112370>, 2021.

676 Li, M., Hu, M., Du, B., Guo, Q., Tan, T., Zheng, J., Huang, X., He, L., Wu, Z., Guo, S.: Temporal and
677 spatial distribution of PM_{2.5} chemical composition in a coastal city of Southeast China, *Sci. Total*
678 *Environ.*, 605-606, 337-346, <https://doi.org/10.1016/j.scitotenv.2017.03.260>, 2017a.

679 Li, M., Liu, H., Geng, G., Hong, C., Liu, F., Song, Y., Tong, D., Zheng, B., Cui, H., Man, H., Zhang, Q.,
680 He, K.: Anthropogenic emission inventories in China: a review, *Natl. Sci. Rev.*, 4, 834-866,
681 <https://doi.org/10.1093/nsr/nwy044>, 2017b.

682 Li, X., He, K., Li, C., Yang, F., Zhao, Q., Ma, Y., Chen, Y., Ouyang, W., Chen, G.: PM_{2.5} mass, chemical
683 composition, and light extinction before and during the 2008 Beijing Olympics, *J. Geophys. Res.*,
684 118, 12158-12167, <https://doi.org/10.1002/2013JD020106>, 2013.

685 Liang, F., Xiao, Q., Yang, X., Liu, F., Li, J., Lu, X., Liu, Y., Gu, D.: The 17-y spatiotemporal trend of
686 PM_{2.5} and its mortality burden in China, *Proc. Natl. Acad. Sci.*, 117, 25601-25608,
687 <https://doi.org/10.1073/pnas.1919641117>, 2020.

688 Lv, L., Wei, P., Li, J., Hu, J.: Application of machine learning algorithms to improve numerical simulation
689 prediction of PM_{2.5} and chemical components, *Atmos. Pollut. Res.*, 12, 101211,
690 [10.1016/j.apr.2021.101211](https://doi.org/10.1016/j.apr.2021.101211), 2021.

691 NBS (National Bureau of Statistics of China): China Statistical Yearbook 2021,
692 <http://www.stats.gov.cn/tjsj/ndsj/2021/indexch.htm>, last access: 2022.

693 Peterson, G., Hogrefe, C., Corrigan, A., Neas, L., Mathur, R., Rappold, A.: Impact of Reductions in
694 Emissions from Major Source Sectors on Fine Particulate Matter–Related Cardiovascular Mortality,
695 *Environ. Health Persp.*, 128, 017005, <https://doi.org/10.1289/EHP5692>, 2020.

696 Qi, H., Cui, C., Zhao, T., Bai, Y., Liu, L.: Numerical simulation on the characteristics of PM_{2.5} heavy
697 pollution and the influence of weather system in Hubei Province in winter 2015 (In Chinese),
698 Meteorological monthly, 45, 1113-1122, <https://doi.org/10.7519/j.issn.1000-0526.2019.08.008>,
699 2019.

700 Seinfeld, J. H., Pandis, S. N.: Atmospheric Chemistry and Physics, from air pollution to climate change.
701 John Wiley & Sons, Inc., Hoboken, New Jersey.47-61, ISBN9781119221166, 2006

702 Sha, T., Ma, X., Jia, H., Tian, R., Chang, Y., Cao, F., Zhang, Y.: Aerosol chemical component: Simulations
703 with WRF-Chem and comparison with observations in Nanjing, Atmos. Environ., 218, 1-14,
704 <https://doi.org/10.1016/j.atmosenv.2019.116982>, 2019.

705 Shi, W., Liu, C., Norback, D., Deng, Q., Huang, C., Qian, H., Zhang, X., Sundell, J., Zhang, Y., Li, B.,
706 Kan, H., Zhao, Z.: Effects of fine particulate matter and its constituents on childhood pneumonia: a
707 cross-sectional study in six Chinese cities, Lancet, 392, S79, <https://doi.org/10.1016/S0140->
708 6736(18)32708-9, 2018.

709 Shi, Z., Li, J., Huang, L., Wang, P., Wu, L., Ying, Q., Zhang, H., Lu, L., Liu, X., Liao, H., Hu, J.: Source
710 apportionment of fine particulate matter in China in 2013 using a source-oriented chemical transport
711 model, Sci. Total Environ., 601-602, 1476-1487, <https://doi.org/10.1016/j.scitotenv.2017.06.019>,
712 2017.

713 Song, S. Y., Wang, Y. S., Wang, Y. L., Wang, T., Tan, H. Z.: The characteristics of particulate matter and
714 optical properties of Brown carbon in air lean condition related to residential coal combustion,
715 Powder Technol., 379, 505-514, <https://doi.org/10.1016/j.powtec.2020.10.082>, 2021.

716 Tang, X. Y., Zhang, Y. H., Shao, M.: Atmosphere Environment Chemistry, Second ed (In Chinese). .
717 Higher Education Press, Beijing, China.268-329, ISBN978-7-04-019361-9, 2006

718 Wang, C., Zheng, J., Du, J., Wang, G., Klemes, J., Wang, B., Liao, Q., Liang, Y.: Weather condition-
719 based hybrid models for multiple air pollutants forecasting and minimisation, J. Clean. Prod., 352,
720 131610, <https://doi.org/10.1016/j.jclepro.2022.131610>, 2022.

721 Wang, D., Hu, J., Xu, Y., Lv, D., Xie, X., Kleeman, M., Xing, J., Zhang, H., Ying, Q.: Source
722 contributions to primary and secondary inorganic particulate matter during a severe wintertime
723 PM_{2.5} pollution episode in Xi'an, China, Atmos. Environ., 97, 182-194,
724 <https://doi.org/10.1016/j.atmosenv.2014.08.020>, 2014.

725 Weagle, C., Sinder, G., Li, C. C., Donkelaar, A., S, P., Bissonnette, P., Burke, I., Jackson, J., Latimer, R.,
726 Stone, E., Abboud, I., Akoshile, C., Anh, N., Brook, J., Cohen, A., Dong, J., Gibson, M., Griffith,
727 D., He, K., Holben, B., Kahn, R., Keller, C., Kim, J., Lagrosas, N., Lestari, P., Khian, Y., Liu, Y.,
728 Marais, E., Martins, J., Misra, A., Muliane, U., Pratiwi, R., Quel, E., Salam, A., Segey, L., Tripathi,
729 S., Wang, C., Zhang, Q., Brauer, M., Rudich, Y., Martin, R.: Global Sources of Fine Particulate
730 Matter: Interpretation of PM_{2.5} Chemical Composition Observed by SPARTAN using a Global
731 Chemical Transport Model, Environ. Sci. Technol., 52, 11670-11681,
732 <https://doi.org/10.1021/acs.est.8b01658>, 2018.

733 Wongphatarakul, V., Friedlander, S. K., Pinto, J. P.: A Comparative Study of PM_{2.5} Ambient Aerosol
734 Chemical Databases, Environ. Sci. Technol., 32, 3926-3934, <https://doi.org/10.1021/es9800582>,
735 1998.

736 Wu, B., Bai, X., Liu, W., Zhu, C., Hao, Y., Lin, S., Liu, S., Luo, L., Liu, X., Zhao, S., Hao, J., Tian, H.:
737 Variation characteristics of final size-segregated PM emissions from ultralow emission coal-fired
738 power plants in China, Environ. Pollut., 259, 113886, <https://doi.org/10.1016/j.envpol.2019.113886>,
739 2020.

740 Wu, D., Zheng, H., Li, Q., Jin, L., Lyu, R., Ding, X., Huo, Y., Zhao, B., Jiang, J., Chen, J., Li, X., Wang,
741 S.: Toxic potency-adjusted control of air pollution for solid fuel combustion, *Nat. Energy*, 7, 194-
742 202, <https://doi.org/10.1038/s41560-021-00951-1>, 2022.

743 Wu, Z. X., Hu, T. F., Hu, W., Shao, L. Y., Sun, Y. Z., Xue, F. L., Niu, H. Y.: Evolution in physicochemical
744 properties of fine particles emitted from residential coal combustion based on chamber experiment,
745 *Gondwana Res.*, <https://doi.org/10.1016/j.gr.2021.10.017>, 2021.

746 Xia, Z. Q., Fan, X. L., Huang, Z. J., Liu, Y. C., Yin, X. H., Ye, X., Zheng, J. Y.: Comparison of Domestic
747 and Foreign PM_{2.5} Source Profiles and Influence on Air Quality Simulation (In Chinese), *Res.*
748 *Environ. Sci.*, 30, 359-367, <https://doi.org/10.13198/j.issn.1001-6929.2017.01.55>, 2017.

749 Yang, F., Tan, J., Zhao, Q., Du, Z., He, K., Ma, Y., Duan, F., Chen, G., Zhao, Q.: Characteristics of PM_{2.5}
750 speciation in representative megacities and across China, *Atmos. Chem. Phys.*, 11, 1025-1051,
751 <https://doi.org/10.5194/acpd-11-1025-2011>, 2011.

752 Ying, Q., Feng, M., Song, D. L., Wu, L., Hu, J., Zhang, H., Kleeman, M., Li, X.: Improve regional
753 distribution and source apportionment of PM_{2.5} trace elements in China using inventory-observation
754 constrained emission factors, *Sci. Total Environ.*, 624, 355-365,
755 <https://doi.org/10.1016/j.scitotenv.2017.12.138>, 2018.

756 Yu, Z. C., Jang, M., Kim, S., Bae, C., Koo, B., Beardsley, R., Park, J., Chang, L., Lee, H., Lim, Y., Cho,
757 J.: Simulating the Impact of Long-Range-Transported Asian Mineral Dust on the Formation of
758 Sulfate and Nitrate during the KORUS-AQ Campaign, *Earth Space Chem.*, 4, 1039-1049,
759 <https://doi.org/10.1021/acsearthspacechem.0c00074>, 2020.

760 Zhang, J., Wu, J., Lv, R., Song, D., Huang, F., Zhang, Y., Feng, Y.: Influence of Typical Desulfurization
761 Process on Flue Gas Particulate Matter of Coal-fired Boilers (In Chinese), *Environ. Sci.*, 41, 4455-
762 4461, <https://doi.org/10.13227/j.hjcx.202003193>, 2020.

763 Zhang, Q., Xue, D., Wang, S., Wang, L., Wang, J., Ma, Y., Liu, X.: Analysis on the evolution of PM_{2.5}
764 heavy air pollution process in Qingdao (In Chinese), *China Environ. Sci.*, 37, 3623-3635,
765 <https://doi.org/10.3969/j.issn.1000-6923.2017.10.003>, 2017.

766 Zhang, S. P., Xing, J., Sarwar, G., Ge, Y. L., He, H., Duan, F., Zhao, Y., He, K., Zhu, L., Chu, B.:
767 Parameterization of heterogeneous reaction of SO₂ to sulfate on dust with coexistence of NH₃ and
768 NO₂ under different humidity conditions, *Atmos. Environ.*, 208, 133-140,
769 <https://doi.org/10.1016/j.atmosenv.2019.04.004>, 2019.

770 Zheng, B., Tong, D., Li, M., Liu, F., Hong, C., Geng, G., Li, H., Li, X., Peng, L., Qi, J., Yan, L., Zhang,
771 Y., Zhao, H., Zheng, Y., He, K., Zhang, Q.: Trends in China's anthropogenic emissions since 2010
772 as the consequence of clean air actions, *Atmos. Chem. Phys.*, 18, 14095-14111,
773 <https://doi.org/10.5194/acp-18-14095-2018>, 2018.

774 Zheng, B., Zhang, Q., Zhang, Y., He, K. B., Wang, K., Zheng, G. J., Duan, F. K., Ma, Y. L., Kimoto, T.:
775 Heterogeneous chemistry: a mechanism missing in current models to explain secondary inorganic
776 aerosol formation during the January 2013 haze episode in North China, *Atmos. Chem. Phys.*, 15,
777 2031-2049, <https://doi.org/10.5194/acp-15-2031-2015>, 2015.

778 Zheng, H., Song, S., Sarwar, G., Gen, M., Wang, S., Ding, D., Chang, X., Zhang, S., Xing, J., Sun, Y. L.,
779 Ji, D., Chan, C. K., Gao, J., McElroy, M.: Contribution of Particulate Nitrate Photolysis to
780 Heterogeneous Sulfate Formation for Winter Haze in China, *Environ. Sci. Technol. Lett.*, 7, 632-
781 638, <https://doi.org/10.1021/acs.estlett.0c00368>, 2020.

782 Zhou, L., Chen, X., Tian, X.: The impact of fine particulate matter (PM_{2.5}) on China's agricultural
783 production from 2001 to 2010, *J. Clean. Prod.*, 178, 133-141,

784 <https://doi.org/10.1016/j.jclepro.2017.12.204>, 2018.

785